Progress In Electromagnetics Research, Vol. 126, 185–201, 2012

FAST ANTENNA CHARACTERIZATION USING THE SOURCES RECONSTRUCTION METHOD ON GRAPHICS PROCESSORS

J. A. López-Fernández*, M. López-Portugués, Y. Álvarez, C. García, D. Martínez-Álvarez, and F. Las-Heras

Universidad de Oviedo, Área de Teoría de la Señal y Comunicaciones, Campus Universitario, Edificio Polivalente, Gijón 33203, Spain

Abstract—The Sources Reconstruction Method (SRM) is a non-invasive technique for, among other applications, antenna characterization. The SRM is based on obtaining a distribution of equivalent currents that radiate the same field as the antenna under test. The computation of these currents requires solving a linear system, usually ill-posed, that may be very computationally demanding for commercial antennas. Graphics Processing Units (GPUs) are an interesting hardware choice for solving compute-bound problems that are prone to parallelism. In this paper, we present an implementation on GPUs of the SRM applied to antenna characterization that is based on a compute-bound algorithm with a high degree of parallelism. The GPU implementation introduced in this work provides a dramatic reduction on the time cost compared to our CPU implementation and, in addition, keeps the low-memory footprint of the latter. For the sake of illustration, the equivalent currents are obtained on a base station antenna array and a helix antenna working at practical frequencies. Quasi real-time results are obtained on a desktop workstation.

1. INTRODUCTION

The radiation pattern of an antenna is a fundamental step for antenna characterization and diagnosis. Due to size limitations, the measurement of the radiation pattern of an antenna on an anechoic chamber is not always possible. In recent years, some methods to compute the radiation pattern of the Antenna Under Test (AUT)

Received 14 December 2011, Accepted 22 February 2012, Scheduled 14 March 2012
* Corresponding author: Jesus A. Lopez-Fernandez (jelofer@tsc.uniovi.es).

by means of a transformation from the Near Field (NF), typically measured in an anechoic chamber, to the Far Field (FF) have been developed [12, 15, 22–24, 31].

Some of the above-mentioned techniques are based on the wave mode expansion, in which the fields radiated by the AUT are expanded in terms of planar, cylindrical, or spherical wave modes and the measured NFs are used to determine the coefficients of the wave modes [12, 31]. The wave mode expansion techniques are limited to canonical acquisition surfaces and the NF-FF transformations are limited to the same type of surface than that of the acquisition one. As a consequence, the computation of the field over a surface that has a different shape than the acquisition one may considerably increase the computational cost. In addition, the NF-FF transformations that these methods use are based on Fast Fourier Transform (FFT) calculations and, consequently, this imposes a minimum spatial sampling rate of the measured field to satisfy Nyquist criterion [31], although recent advances in NF-FF transformations are able to overcome this limitation, thus reducing the number of sampling points to be employed [8, 9]. Another drawback of the planar and cylindrical wave mode expansion techniques is due to the truncation or windowing of the fields that are assumed to be zero outside of the acquisition domain [22]. Nonetheless, the use of the FFT algorithm makes these methods very computationally efficient which represents their main advantage [2].

An alternative to wave mode expansion technique is the Sources Reconstruction Method (SRM) that is based on obtaining, from the measured field (usually NF, although not limited to), an equivalent distribution of currents that radiate the same field, outside the source domain, as that of the AUT [15, 22–24]. The SRM and a method based on the relationship between spherical and planar wave modes are compared for antenna diagnostics in [16].

The equivalent currents distribution are determined from the measured field by solving an integral equation, relating fields and sources through the vector potentials [7], that may be used when the original problem is posed in terms of the electromagnetic Equivalence Principle [7]. The equivalent problem may be characterized from the electric and magnetic equivalent currents expressed in terms of a canonical 3-D coordinate system. Nonetheless, the numerical performance of this approach is deteriorated because it requires additional conditions to force that the currents are tangential to the surface [1]. A more convenient formulation to model the equivalent currents is presented in [15] where a coordinate system over each facet, based on two tangential and orthogonal unit vectors, is defined to express the components of both the electric and magnetic equivalent

currents. In [24] the accuracy of the SRM is improved by means of a formulation based on a dual integral equation. The accuracy of the most common formulation based on a single integral equation is compared to the one of the dual integral equation in [25].

The SRM does not impose any geometrical restriction to the acquisition and reconstruction domains [5, 14, 21, 24] which enlarges its scope of application beyond antenna characterization and diagnostics. For instance, in [14] the SRM is used to obtain the exclusion zones for human exposure of transmitting antennas and in [21] the equivalent currents are computed on a radome to improve its design.

The main drawback of the SRM is the computational cost associated to the calculation of the equivalent currents for electrically large antennas [2]. The integral equation relating fields and currents is discretized, usually by the Method of Moments (MoM), yielding a linear system of M equations and N unknowns, where M is proportional to the number of acquisition points and N is proportional to the number of basis functions that expand the equivalent currents. Iterative solvers, such as the Conjugated Gradient method for minimizing the Norm of the Residual (CGNR) [30], are commonly used to obtain the unknown currents from the mentioned linear system. The iterative solver requires some Matrix-Vector Products (MVPs) per iteration and, in most cases, several iterations to achieve the desired accuracy on the equivalent currents.

Different efficient algorithms based on acceleration methods for direct problems have been increasing the capability of characterizing electrically large antennas by reducing the computational cost of the solver. For instance, in [3] the single level Fast Multipole Method (FMM) is used to speed up the solution of the system. The Multilevel FMM (MLFMM) for the SRM was later introduced by [10] and used in combination with higher order basis functions in [11]. It is also worth mentioning the computational efficiency achieved by the Adaptive Cross Approximation algorithm (ACA) approach for the SRM [4, 33] and by its multilevel version [28]. All these approaches make use of the available memory resources in order to reduce the calculation time. In contrast with these techniques, the Memory-Saving Technique (MST) introduced in [15] avoids the storage of the impedance matrix by calculating its rows only when required to perform the MVP. The use of the MST yields a dramatic reduction on the memory requirements compared to any other of the above-mentioned efficient algorithms (FMM or ACA). The drawback of the MST is that it appreciably increases the calculation time due to the computation of the system matrix at every iteration.

Parallel computing applied to solving electromagnetic problems

is broadly spread [6, 27, 32]. Among the growing number of parallel hardware, the Graphics Processing Units (GPUs) may be considered the most outstanding architecture, since they offer massive computing capabilities and they are widely deployed. In fact, the GPUs are a very interesting choice for those compute-bound algorithms that pose a high degree of parallelism and a low memory footprint [20]. As a consequence, the GPUs seem to be a very convenient framework for the implementation of the SRM using the MST.

In this paper, we describe an implementation of the SRM using GPUs. We use the CGNR to iteratively solve the linear system of equations posed by the MoM. In addition, we adapt the MST to the GPU architecture to compute the elements of the impedance matrix on the fly. A remarkable speedup, compared to CPU implementations (with or without MST), and a very low memory footprint are achieved. This paper is organized as follows. Section 2 is devoted to the mathematical formulation of the SRM that we use in this work. In Section 3, we present our GPU implementation. Some numerical results related to the performance of the developed solver are shown in Section 4. Finally, some conclusions are summarized in Section 5.

2. MATHEMATICAL FORMULATION OF THE SOURCES RECONSTRUCTION METHOD

In this section, we summarize the main foundations of the SRM (see, for instance, [15, 22] for a more detailed description). The SRM is based on the electromagnetic Equivalence Principle [7], which states that given a set of sources bounded by the volume V' operating in free space, the fields (electric and magnetic) generated by the actual sources outside a surface S' (enclosing V') equals the fields radiated by equivalent currents distributed on the surface S' (see Fig. 1). Therefore, the goal is the AUT characterization by means of a distribution of equivalent electric ($\overrightarrow{J}_{eq}$) and magnetic currents ($\overrightarrow{M}_{eq}$) that radiate, outside S', the same field as the AUT ($\overrightarrow{E}_2, \overrightarrow{H}_2$).

The equivalent currents may be related to the electromagnetic field at any point outside S' by means of integral equations using the vector potentials [7]. In this manner, the equivalent currents may be retrieved from the measured field on the acquisition domain (outside S', see Fig. 1) and then, the field at any point may be determined from these currents. The knowledge of just one field (electric or magnetic) is enough for the calculation of both equivalent currents ($\overrightarrow{J}_{eq}$ and $\overrightarrow{M}_{eq}$, see Fig. 1(b)) and the formulation of the SRM based on one field acquisition is dual to the formulation based on the other [17].

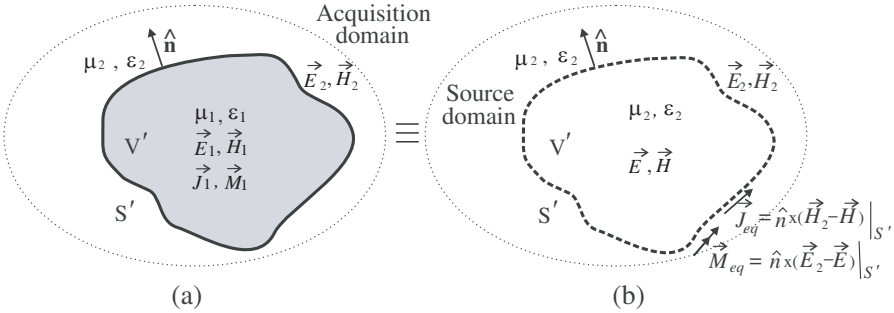

Figure 1. Illustration of the Equivalence Principle. (a) Real problem. (b) Equivalent problem.

In addition, the knowledge of the tangential components of the field on a closed acquisition domain is enough to accurately determine the tangential equivalent currents and, in consequence, the total field at any point of the space outside the source domain [17].

2.1. Integral Equations

Since the medium in the equivalent problem is homogeneous it is possible to use the Green's function methodology (or the vector potentials) that expresses the total electric field at any observation point $\overrightarrow{r} \notin V'$ by the superposition of the contributions due to the electric and magnetic current distributions:

$$\overrightarrow{E}(\overrightarrow{r}) = \overrightarrow{E}_J(\overrightarrow{r}) + \overrightarrow{E}_M(\overrightarrow{r}), \tag{1}$$

$$\overrightarrow{E}_J(\overrightarrow{r}) = -\frac{j\eta}{4\pi k}\int_{S'}\left\{\left(k^2+\nabla^2\right)\left[\overrightarrow{J}_{eq}(\overrightarrow{r}')\, g(\overrightarrow{r},\overrightarrow{r}')\right]\right\} \mathrm{d}S', \tag{2}$$

$$\overrightarrow{E}_M(\overrightarrow{r}) = -\frac{1}{4\pi}\nabla\times\int_{S'}\left[\overrightarrow{M}_{eq}(\overrightarrow{r}')\, g(\overrightarrow{r},\overrightarrow{r}')\right] \mathrm{d}S', \tag{3}$$

where η is the characteristic impedance of the medium, k is the wavenumber, $\overrightarrow{r}'$ is the vector defining the source point. $\overrightarrow{J}_{eq}(\overrightarrow{r}')$ and $\overrightarrow{M}_{eq}(\overrightarrow{r}')$ are the equivalent electric and magnetic current distribution, respectively, defined on the surface S'. In addition, $g(\overrightarrow{r},\overrightarrow{r}')$ is the free space Green's function on an observation point $\overrightarrow{r}$ associated to a source point placed at $\overrightarrow{r}'$, defined as follows:

$$g(\overrightarrow{r},\overrightarrow{r}') = \frac{e^{-jk|\overrightarrow{r}-\overrightarrow{r}'|}}{4\pi|\overrightarrow{r}-\overrightarrow{r}'|} \tag{4}$$

2.2. Numerical Solution of the Integral Equations

In this work, we use the MoM to formulate the integro-differential equations involved in Equation (1). We need to expand the unknown currents in terms of some known basis functions multiplied by unknown constants. For the sake of simplicity, Pulse Basis Functions (PBFs) are considered in the sequel. A solver for the SRM that uses Rao, Wilton, and Glisson (RWG) basis functions [26] is presented in [17]. We also consider a spherical range (spherical acquisition surface) which is a typical configuration for antenna measurement setup in anechoic chamber.

Considering a spherical acquisition domain and a local coordinate system at each facet of surface S' in the manner (u, v, n) with $\widehat{u}$ and $\widehat{v}$ two orthogonal unit vectors tangential to the surface and $\widehat{n}$ the outward normal unit vector, it is possible to relate the field and the currents by means of impedance matrixes as follows:

$$\begin{bmatrix} E_\theta \\ E_\varphi \end{bmatrix} = \begin{bmatrix} Z_{\theta,\,J_u} & Z_{\theta,\,J_v} \\ Z_{\varphi,\,J_u} & Z_{\varphi,\,J_v} \end{bmatrix} \begin{bmatrix} J_u \\ J_v \end{bmatrix} + \begin{bmatrix} Z_{\theta,\,M_u} & Z_{\theta,\,M_v} \\ Z_{\varphi,\,M_u} & Z_{\varphi,\,M_v} \end{bmatrix} \begin{bmatrix} M_u \\ M_v \end{bmatrix} \tag{5}$$

that may be expressed in a more compact form as follows:

$$[E] = [Z_J]\,[J] + [Z_M]\,[M] \tag{6}$$

The elements of matrixes $[Z_J]$ and $[Z_M]$ have very different root mean square values which worsens the conditioning of the linear system. In order to improve the conditioning of the system and, thus, the convergence of the iterative solver, it is possible to define the normalized equations [15] that ensures that all the terms have a similar weight in the system:

$$\overline{[E]} = \overline{[Z_J]}\,\overline{[J]} + \overline{[Z_M]}\,\overline{[M]} \tag{7}$$

where the normalization for a general matrix A of order $M \times N$ is defined as follows:

$$\overline{[A]} = \frac{1}{\mathrm{RMS}\left([A]\right)}\,[A] \tag{8}$$

where:

$$\mathrm{RMS}\,[A] = \frac{\|\,[A]\,\|_F}{\sqrt{NM}} = \sqrt{\frac{\displaystyle\sum_{n=1}^{N}\sum_{m=1}^{M} |a_{m,\,n}|^2}{NM}} \tag{9}$$

Note that $\|\,[A]\,\|_F$ notes the Frobenius norm of matrix $[A]$ and, thus, $a_{m,\,n}$ is the m-row and n-column element of $[A]$.

Once equivalent currents distributions $\overline{[J]}$ and $\overline{[M]}$ are obtained the unnormalized corresponding magnitudes are retrieved using:

$$[J] = \frac{\text{RMS}([E])}{\text{RMS}([Z_J])}\overline{[J]} \tag{10}$$

$$[M] = \frac{\text{RMS}([E])}{\text{RMS}([Z_M])}\overline{[M]} \tag{11}$$

The linear system presented in Equation (7) is generally ill-posed due to the nature of the inverse problem to be solved (in this case, the equivalent currents retrieval from the radiated fields). In addition, the impedance matrixes may be very large for arbitrary AUT geometries. We use the CGNR [30] to solve Equation (7) which provides a kind of least mean squares solution. The cost function minimized by the CGNR is related to the difference between the measured field and the field radiated by the reconstructed currents. We have chosen an iterative solver because it permits to compute the impedance matrix on the fly (for instance, using the MST [15]) avoiding its storage and, thus, yielding a very low memory footprint.

3. PARALLEL ALGORITHM AND GPU IMPLEMENTATION

The computation associated to the MVP of each CGNR iteration has a time cost $O(MN)$. In addition, the impedance matrix must be calculated on each iteration if its storage is avoided. Nevertheless, all these numerous complex computations may be accomplished in parallel as long as we properly tackle the problem. Thus the original algorithm must be carefully modified to exploit the underlying GPU hardware.

We decided to use NVIDIA CUDA (Compute Unified Device Architecture) [19] to deal with the GPU. In addition, we use a fine grain approach that perfectly matches the SIMT paradigm (Single Instruction Multiple Threads) [18]. In this manner, we divide the problem into many sub-problems that may be calculated independently using thousands or even millions of threads, depending on the problem size. Such a large number of threads (much more than the available cores) allows to hide the memory latency and, therefore, is common in GPU programming [19].

Figure 2 plots an example to explain the strategy (cyclic-checkerboard partitioning) that we use to parallelize the calculation of the MVP. This technique entails a 2D division where matrix rows are assigned to CUDA blocks [19] and columns are assigned to CUDA threads, both of them in a cyclic fashion. Note that matrix elements are computed on the fly and not permanently stored, neither in CPU nor

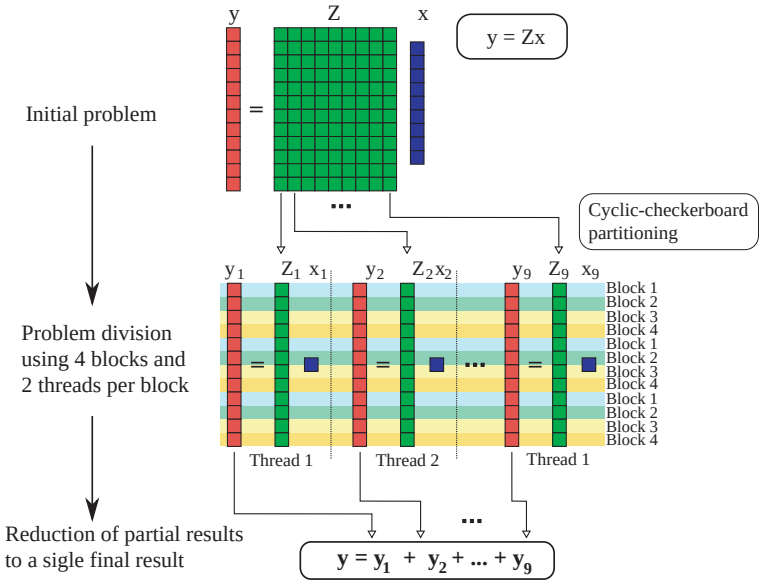

Figure 2. Example to illustrate our parallel MVP implementation.

in GPU memory. As a result, we have obtained a parallelized MVP with minimum memory requirements that fits the massively parallel architecture of the GPU.

Our implementation of the SRM for GPUs consists of several kernels, half of which are used to deal with electric currents and the other half with magnetic currents. It is interesting to note that we try to use the GPU registers (fastest memory) as much as possible to perform the calculations, in order to minimize memory-access latency. In addition, accesses to arrays are both aligned and sequential, which improves transactions from GPU memory [19]. Moreover, in order to develop an appropriate algorithm for CUDA, we must also take into consideration that only the threads within a given block can access (read or write) the same shared-memory block [19]. Therefore, prior to obtain the solution vector, we have to perform a reduction per block, in which all threads that pertain to the same block collaborate to add their partial contributions. Each reduction entails a time cost of only $O(\log_2(threads\_per\_block))$ and, in addition, several of them may be done in parallel.

In Table 1, we show the parameters that yield the best performance for the developed kernels in our numerical experiments. Since the highest amount of shared memory per block is under 16 KB,

Table 1. Configuration parameters for the CUDA kernels.

Grid size (*number of blocks*)	8192
Block size (*threads per block*)	128
Shared memory (*usage per block*)	2 KB–2.5 KB (kernel dependent)
Registers (*usage per thread*)	63

we decided to run all the kernels with L1 cache preference. That is, 16 KB of shared memory and 48 KB of L1 cache per multiprocessor. In this manner, we may benefit from the high amount of L1 cache in those data-dependent memory accesses and, at the same time, we can use some shared memory to perform the reduction of the solution vector.

4. NUMERICAL EXPERIMENTS

In this section, we compute the equivalent currents over a base station antenna and a helix antenna using different implementations of the SRM. In the experiments shown in here, the CGNR iteratively solves the linear system posed by the SRM until the Root Mean Square Error (RMSE) between the measured field and the field radiated by the equivalent currents reaches the 5%.

In order to obtain the equivalent currents over the AUTs, we have used a workstation that consists of 2 dual-core CPUs (AMD Opteron 265 at 1.8 GHz), 16 GB of RAM, and 1 NVIDIA GTX 460 GPU (336 cores and 1 GB GDDR5). We have compiled the CPU source codes and the GPU CUDA codes by means of Intel icc 11.1 and of NVIDIA nvcc 3.2, respectively. We have used OpenMP [29] to provide shared memory parallelism in CPU codes. In addition, single precision arithmetic is utilized in all codes.

4.1. Base Station Antenna

This application example reviews the one presented in [2]. The goal is computing the equivalent currents over a Base Transceiver Station (BTS) antenna array working at 1.8 GHz. The electric field has been measured at the spherical range in an anechoic chamber (see Fig. 3(a)). The distance between the AUT and the probe (horn antenna) is 5 m (30λ).

Whenever the far field distance R_{FF} for an antenna is much greater than the wavelength and than the antenna size ($R_{\mathrm{FF}} \gg \lambda$ and $R_{\mathrm{FF}} \gg D_0$) then R_{FF} may be expressed from the physical size of

the antenna D_0 as follows [12, 34]:

$$R_{\mathrm{FF}} = 2\frac{(D_0)^2}{\lambda} \tag{12}$$

Otherwise the far field distance is given by the most restrictive condition ($R_{\mathrm{FF}} \geq \max\{10\lambda, 10D_0\}$). Since the physical size of the BTS is $D_0 = 2\,\mathrm{m}$, the FF distance is, following Equation (12), $R_{\mathrm{FF}} = 48\,\mathrm{m}$. Therefore, the BTS has been measured in its NF region. According to the developments shown in [12] (pp. 189–190) the minimum sampling rate for this antenna is $\Delta\theta \approx \Delta\varphi \approx 3.75^\circ$. In order to ensure a proper sampling, we used an angular sampling rate of $\Delta\theta = 1^\circ$ and $\Delta\varphi = 3^\circ$, yielding 21901 field samples.

The equivalent currents domain fits the radome that covers the AUT surface and consists of 1910 patches (mesh size about 0.15λ). In consequence, the system of equations to be solved has 43802 equations (21901 field samples for each field component, E_θ and E_φ) and 7640 unknowns (1910 unknowns for each component of the electric current, J_u and J_v, and for each component of the magnetic current, M_u and M_v).

The problem has been solved using 4 OpenMP threads and three different implementations: CPU-only implementation storing the impedance matrix (Non MST+CPU) and the MST for both CPU-only (MST + CPU) and CPU-GPU (MST + CPU-GPU) implementations. Table 2 summarizes the main computational cost parameters for these implementations.

As pointed out in Table 2, the GPU implementation allows solving the problem in almost real time (3 s) and the speedup is 90 times with respect to the MST + CPU implementation of the SRM. It is worth comparing the memory consumption of the implementations that recalculate the impedance matrix at each iteration (around 5

Table 2. Comparison of the computational cost associated to different implementations of the SRM used to obtain the equivalent currents on the BTS antenna.

Parameter	Non MST + CPU	MST + CPU	MST + CPU-GPU
Memory [MB]	5100	5	4
Z calculation [s]	21		
CGNR it. time [s]	5.6	27	0.3
Execution time [s]	77	270	3
Field RMSE %	3.4	3.4	3.4
Number of iterations	10	10	10

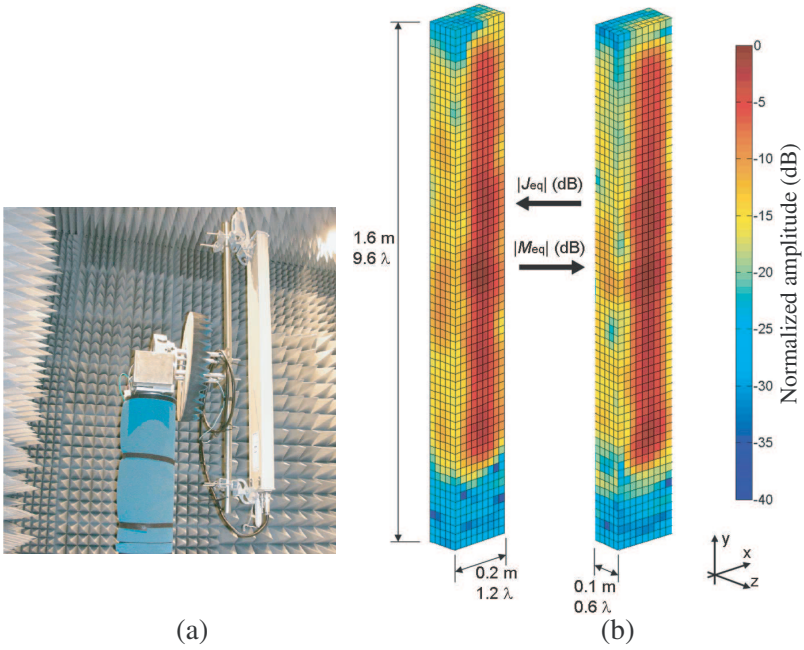

Figure 3. (a) BTS antenna and antenna measurement system at the spherical range in the anechoic chamber. (b) Reconstructed equivalent electric and magnetic currents on the radome enclosing the BTS antenna (normalized amplitude, in dB).

MBytes) with the one that stores the impedance matrix (more than 5 GBytes for this moderate size problem). Nonetheless, the storage of the matrix yields a reduction on the iteration time about 5 times (5.6 s instead of 27 s). In terms of execution time, the proposed MST + CPU-GPU implementation is 25 times faster than the CPU-only fastest implementation (Non MST + CPU).

The BTS antenna and the measurement system are plotted in Fig. 3(a) and the normalized amplitude of the reconstructed equivalent currents on its surface are depicted in Fig. 3(b).

4.2. Helix Antenna

In this case, we want to obtain the equivalent currents over a helix antenna (see Fig. 4(a)) working at 4.5 GHz. The electric field has been measured at the spherical range in an anechoic chamber. The distance between the AUT and the probe is 4.85 m (72.75λ).

The physical size of the AUT is $D_0 = 0.2$ m and $\lambda = 0.067$ m, so the far field distance for this antenna is, following the discussion

about Equation (12), $R_{\mathrm{FF}} = 2\,\mathrm{m}$. Thus, the AUT has been measured in its FF region. For this antenna, the minimum sampling rate is $\Delta\theta \approx \Delta\varphi \approx 9^\circ$ [12]. A sampling rate of $\Delta\theta = 1^\circ$ and $\Delta\varphi = 3^\circ$ has been chosen to ensure a proper sampling. Thus, the number of field samples is the same as in the BTS example (21901).

The equivalent currents domain fits the radome that covers the AUT surface and consists of 20640 patches (mesh size about 0.05λ). In consequence, the system of equations to be solved has 43802 equations (21901 field samples for each field component, E_θ and E_φ) and 82560 unknowns (20640 unknowns for each component of the electric current, J_u and J_v, and for each component of the magnetic current, M_u and M_v). The resulting system of equations is underdetermined. However, as indicated in previous works [5, 14, 21, 24], the SRM seeks a least-mean-square solution, that is, the minimum energy solution. The issue of solution uniqueness of the inverse problem for antenna characterization has been widely discussed in [13, 24, 25], as well as the different ways of Equivalence Principle application depending whether the zero internal field condition is enforced or not.

In this case, the storage of the impedance matrix would require up to 55 GBytes that exceeds the workstation memory. As a consequence, we have solved the problem using the MST for both CPU-only and CPU-GPU implementations with 4 OpenMP threads. Table 3

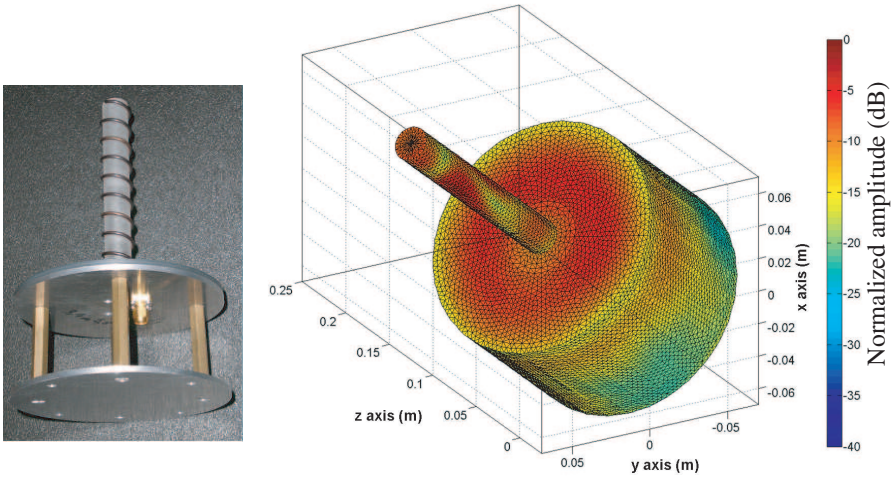

(a) (b)

Figure 4. (a) Helix antenna to be characterized. (b) Reconstructed equivalent electric currents on the surface enclosing the helix antenna (normalized amplitude, in dB).

Table 3. Comparison of the computational cost of CPU-only and CPU-GPU implementations for the helix antenna.

Parameter	MST + CPU	MST + CPU-GPU
Memory [MB]	10	8
CGNR iteration time [s]	220	2.9
Execution time [s]	1980	26
Convergence %	3.9	3.9
Number of iterations	9	9

summarizes the main calculation parameters. It is worth noting again the speedup of the CPU + GPU implementation against the CPU-only one (76 times).

The helix antenna is depicted in Fig. 4(a) and the normalized amplitude of the reconstructed electric equivalent currents on its surface are depicted in Fig. 4(b). From the reconstructed equivalent currents using the CPU-only and CPU-GPU implementation of the SRM, the far field patterns are calculated. Fig. 5(a) and Fig. 5(b) plot, respectively, the $\varphi = 0°$ and $\varphi = 90°$ cuts of the far field pattern, showing no differences between CPU-only and CPU-GPU based results.

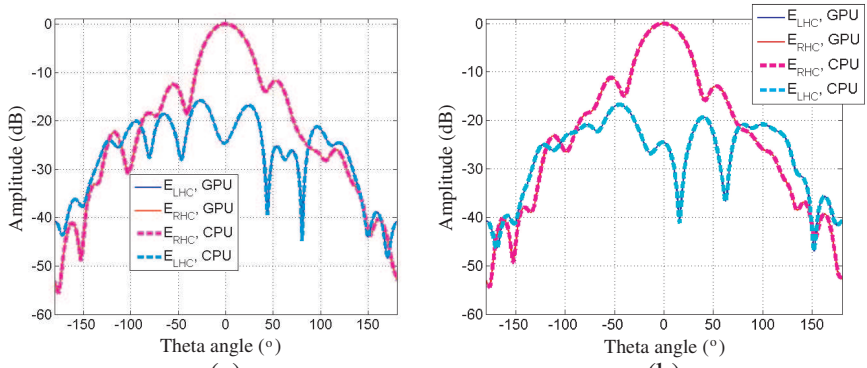

Figure 5. Right handed and left handed circular components of the far field pattern for the helix antenna. (a) Cut corresponding to $\varphi = 0°$. (b) Cut corresponding to $\varphi = 90°$.

5. CONCLUSION

In this work, we present an implementation on GPUs of the SRM applied to the characterization of commercial antennas. In addition, we compare our GPU and CPU implementations using a desktop workstation (4 CPU cores, 16 GB of RAM, 336 GPU cores and 1 GB of GPU memory) for a BTS and for a helix antenna. The results presented in here show that the solution time is reduced about two orders of magnitude when using the whole system (CPU + GPU) instead of only the CPU subsystem. In addition, the GPU implementation keeps the low memory footprint of the CPU implementation that uses the MST. Although a 5x speedup is achieved in the CPU implementation when the impedance matrix is stored, this technique dramatically increases the memory cost and therefore, may not be suitable for some problems (for instance, the helix antenna presented here). Finally, the GPU solver of the SRM presented in this paper provides quasi real-time accurate results for the BTS (3 s) and very reduced time for the helix antenna (26 s).

ACKNOWLEDGMENT

This work has been partially supported by "Ministerio de Ciencia e Innovación" from Spain/FEDER under projects TEC2011-24492/TEC (iSCAT) and CONSOLIDER-INGENIO CSD2008-00068, by "Gobierno del Principado de Asturias" (PCTI)/ FEDER-FSE under projects EQUIP08-06, FC09-COF09-12, EQUIP10-31 and PC10-06, grants BES-2009-024060 and (PCTI) BP11-166, and by Cátedra Telefónica-Universidad de Oviedo.

REFERENCES

1. Álvarez, Y. and F. Las-Heras, "Integral equation algorithms for equivalent currents distribution retrieval over arbitrary three-dimensional surfaces," *IEEE International Symposium on Antennas and Propagation*, 1061–1064, Albuquerque, New Mexico, USA, July 9–14, 2006.
2. Álvarez, Y., F. Las-Heras, and M. R. Pino, "On the comparison between the spherical wave expansion and the sources reconstruction method," *IEEE Transactions on Antennas and Propagation*, Vol. 56, No. 10, 3337–3341, 2008.
3. Álvarez, Y., F. Las-Heras, M. R. Pino, and J. A. López, "Acceleration of the sources reconstruction method via the fast

multipole method," *IEEE International Symposium on Antennas and Propagation*, 1–4, San Diego, California, USA, July 5–11, 2008.

4. Álvarez, Y., F. Las-Heras, and M. R. Pino, "Application of the adaptive cross approximation algorithm to the sources reconstruction method," *3rd European Conference on Antennas and Propagation*, 761–765, Berlin, Germany, March 23–27, 2009.
5. Álvarez, Y., F. Las-Heras, B. A. Casas, and C. García, "Antenna diagnostics using arbitrary-geometry field acquisition domains," *IEEE Antennas and Wireless Propagation Letters*, Vol. 8, 375–378, 2009.
6. Araújo, M. G., J. M. Taboada, F. Obelleiro, J. M. Bértolo, L. Landesa, J. Rivero, and J. L. Rodríguez, "Supercomputer aware approach for the solution of challenging electromagnetic problems," *Progress In Electromagnetics Research*, Vol. 101, 241–256, 2010.
7. Balanis, C. A., *Advanced Engineering Electromagnetics* , John Wiley & Sons, New York, 1989.
8. Capozzoli, A., C. Curcio, G. D'Elia, and A. Liseno, "Singular-value optimization in plane-polar near-field antenna characterization," *IEEE Transactions on Antennas Propagation*, Vol. 52, No. 2, 103–112, 2010.
9. Capozzoli, A., C. Curcio, A. Liseno, and P. Vinetti, "Field sampling and field reconstruction: A new perspective," *Radio Science*, Vol. 45, RS6004, 31, 2010, doi: 10.1029/2009RS004298.
10. Eibert, T. and C. Schmidt, "Multilevel fast multipole accelerated inverse equivalent current method employing Rao-Wilton-Glisson discretization of electric and magnetic surface currents," *IEEE Transactions on Antennas Propagation*, Vol. 57, No. 4, 1178–1185, 2009.
11. Eibert, T. F., Ismatullah, E. Kaliyaperumal, and C. H. Schmidt, "Inverse equivalent surface current method with hierarchical higher order basis functions, full probe correction and multi-level fast multipole acceleration," *Progress In Electromagnetics Research*, Vol. 106, 377–394, 2010.
12. Hansen, J. E., *Spherical Near-field Antenna Measurements*, Vol. 26, Peter Peregrinus Ltd., London, 1988.
13. Inan, K. and R. E. Diaz, "On the uniqueness of the phase retrieval problem from far field amplitude-only data," *IEEE Transactions on Antennas Propagation*, Vol. 59, No. 3, 1053–1057, March 2011.

14. Las-Heras, F., M. R. Pino, S. Loredo, Y. Álvarez, and T. K. Sarkar, "Evaluating near-field radiation patterns of commercial antennas," *IEEE Transactions on Antennas Propagation*, Vol. 54, No. 8, 2198–2207, 2006.
15. López, Y. A., F. Las-Heras, and M. R. Pino, "Reconstruction of equivalent currents distribution over arbitrary three-dimensional surfaces based on integral equation algorithms," *IEEE Transactions on Antennas Propagation*, Vol. 55, No. 12, 3460–3468, 2007.
16. López, Y. A., C. Capellin, F. L. Andrés, and O. Breinbjerg, "On the comparison of the spherical wave expansion-to-plane wave expansion and the sources reconstruction method for antenna diagnostics," *Progress In Electromagnetics Research*, Vol. 87, 245–262, 2008.
17. López, Y. A., F. L. Andrés, M. R. Pino, and T. K. Sarkar, "An improved super-resolution source reconstruction method," *IEEE Transactions on Instrumentation and Measurement*, Vol. 58, No. 11, 3855–3866, 2009.
18. Lindholm, E., J. Nickolls, S. Oberman, and J. Montrym, "NVIDIA Tesla: A unified graphics and computing architecture," *IEEE Micro.*, Vol. 28, No. 2, 39–55, 2008.
19. NVIDIA Corporation, *NVIDIA CUDA C Programming Guide*, ver. 3.2, November 2010, http://developer.download.nvidia.com/.
20. Owens, J. D., M. Houston, D. Luebke, S. Green, J. E. Stone and J. C. Phillips, "GPU computing," *Proceedings of the IEEE*, Vol. 5, No. 96, 879–899, 2008.
21. Persson, K. and M. Gustafson, "Reconstruction of equivalent currents using a near-field data transformation — With radome application," *Progress In Electromagnetics Research*, Vol. 54, 179–198, 2005.
22. Petre, P. and T. K. Sarkar, "Planar near-field to far-field transformation using an equivalent magnetic current approach," *IEEE Transactions on Antennas Propagation*, Vol. 40, No. 11, 1348–1356, 1992.
23. Ponnapalli, S., "Near-field to far-field transformation utilizing the conjugate gradient method," *Progress In Electromagnetics Research*, Vol. 5, 391–422, 1991.
24. Quijano, J. L. A. and G. Vecchi, "Improved-accuracy source reconstruction on arbitrary 3-D surfaces," *IEEE Antennas and Wireless Propagation Letters*, Vol. 8, 1046–1049, 2009.
25. Quijano, J. L. A. and G. Vecchi, "Field and source equivalence in source reconstruction on 3D surfaces," *Progress In Electromag-*

netics Research, Vol. 103, 67–100, 2010.

26. Rao, S. M., D. R. Wilton, and A. W. Glisson, "Electromagnetic scattering by surfaces of arbitrary shape," *IEEE Transactions on Antennas and Propagation*, Vol. 30, No. 3, 409–418, 1982.
27. Taboada, J. M., M. G. Araújo, J. M. Bértolo, L. Landesa, F. Obelleiro, and J. L. Rodríguez, "MLFMA-FFT parallel algorithm for the solution of large-scale problems in electromagnetics," *Progress In Electromagnetics Research*, Vol. 105, 15–30, 2010.
28. Tamayo, J. M., A. Heldring, and J. M. Rius, "Application of multilevel adaptive cross approximation (MLACA) to electromagnetic scattering and radiation problems," *International Conference on Electromagnetics in Advanced Applications*, 178–181, 2009.
29. The OpenMP ARB, *OpenMP*, 2004, www.openmp.org.
30. Wang, H.-C. and K. Hwang, "Multicoloring of grid-structured PDE solvers on shared-memory multiprocessors," *IEEE Transactions on Parallel and Distributed Systems*, Vol. 6, No. 11, 1195–1205, 1995.
31. Yaghjian, A. D., "An overview of near-field antenna measurements," *IEEE Transactions on Antennas Propagation*, Vol. 34, No. 1, 30–45, 1986.
32. Zhang, Y. and T. Sarkar, *Parallel Solution of Integral Equation-Based EM Problems in the Frequency Domain*, John Wiley & IEEE Press, Hoboken, NJ, 2009.
33. Zhao, K., M. N. Vouvakis, and J. F. Lee, "The adaptive cross approximation algorithm for accelerated method of moments computations of EMC problems," *IEEE Transactions on Electromagnetic Compatibility*, Vol. 47, No. 4, 763–773, 2005.
34. Revised IEEE Std 145-1993, "IEEE standard definitions of terms for antennas," *IEEE Transactions on Antennas and Propagation*, Vol. 31-2, 5, 1983.